CANCER IMMUNOLOGY

Targeting latency-associated peptide promotes antitumor immunity

Galina Gabriely,[1] Andre P. da Cunha,[1,2] Rafael M. Rezende,[1] Brendan Kenyon,[1] Asaf Madi,[1] Tyler Vandeventer,[1] Nathaniel Skillin,[1] Stephen Rubino,[1] Lucien Garo,[1] Maria A. Mazzola,[1] Panagiota Kolypetri,[1] Amanda J. Lanser,[1] Thais Moreira,[3] Ana Maria C. Faria,[3] Hans Lassmann,[4] Vijay Kuchroo,[1] Gopal Murugaiyan,[1] Howard L. Weiner[1]*

Regulatory T cells (T_{regs}) promote cancer by suppressing antitumor immune responses. We found that anti-LAP antibody, which targets the latency-associated peptide (LAP)/transforming growth factor–β (TGF-β) complex on T_{regs} and other cells, enhances antitumor immune responses and reduces tumor growth in models of melanoma, colorectal carcinoma, and glioblastoma. Anti-LAP decreases LAP^+ T_{regs}, tolerogenic dendritic cells, and TGF-β secretion and is associated with $CD8^+$ T cell activation. Anti-LAP increases infiltration of tumors by cytotoxic $CD8^+$ T cells and reduces $CD103^+$ CD8 T cells in draining lymph nodes and the spleen. We identified a role for $CD103^+$ CD8 T cells in cancer. Tumor-associated $CD103^+$ CD8 T cells have a tolerogenic phenotype with increased expression of CTLA-4 and interleukin-10 and decreased expression of interferon-γ, tumor necrosis factor–α, and granzymes. Adoptive transfer of $CD103^+$ CD8 T cells promotes tumor growth, whereas CD103 blockade limits tumorigenesis. Thus, anti-LAP targets multiple immunoregulatory pathways and represents a potential approach for cancer immunotherapy.

INTRODUCTION

Classic $CD4^+$ regulatory T cells (T_{regs}) are identified by the intracellular marker Foxp3 (*1*, *2*). However, targeting classic T_{regs} for treatment in humans is hampered by the expression of Foxp3 and surface T_{reg} markers on activated cells. Other types of T_{regs} have also been described, including T regulatory 1 (Tr1) and T helper 3 cells (Th3) (*3*, *4*), although they are not as well understood or characterized as classic $Foxp3^+$ T_{regs}. We have been interested in T_{regs} that express transforming growth factor–β (TGF-β) on their surface forming a complex with latency-associated peptide (LAP), which identifies $CD4^+$ T_{regs} that have been described in the models of oral tolerance and autoimmunity (*3*, *5*, *6*) and are increased in cancer. In colorectal cancer (CRC), LAP^+ CD4 tumor-infiltrating lymphocytes (TILs) are 50-fold more suppressive than $FOXP3^+$ CD4 T cells (*7*). In head and neck cancer, LAP is up-regulated in $FOXP3^+$ CD4 T lymphocytes (*8*). TGF-β is secreted in the tumor microenvironment by different cells and has an important role in dampening the antitumor immune response (*9*, *10*). In cancer, TGF-β controls cell growth, induces angiogenesis and tumor cell invasion, and promotes immunosuppression (*11*). LAP and TGF-β are translated as one precursor polypeptide from the *Tgfb1* gene that undergoes cleavage by furin, which separates the N-terminal LAP protein portion from TGF-β. TGF-β is then reassembled with LAP to form a small latent complex (SLC) that retains TGF-β in its inactive form on the cell surface. The SLC is then deposited on the cell surface bound to the LAP membrane receptor GARP (glycoprotein A repetitions predominant) or embedded in the extracellular matrix (*12*–*14*). We used anti-LAP antibodies that we developed (*15*) to investigate LAP targeting as cancer immunotherapy.

[1]Ann Romney Center for Neurologic Diseases, Evergrande Center for Immunologic Diseases, Brigham and Women's Hospital, Harvard Medical School, Boston, MA 02115, USA. [2]Novartis Institutes for BioMedical Research, Cambridge, MA 02139, USA. [3]Department of Biochemistry and Immunology, Institute of Biological Sciences, Federal University of Minas Gerais, Belo Horizonte 31.270-901, Brazil. [4]Center for Brain Research, Medical University of Vienna, Spitalgasse 4, A-1090 Wien, Austria.
*Corresponding author. Email: hweiner@rics.bwh.harvard.edu

RESULTS

Anti-LAP monoclonal antibody decreases tumor growth in models of melanoma, glioblastoma, and colorectal carcinoma

We used a mouse anti-LAP monoclonal antibody (mAb) (*15*) in orthotopic and flank syngeneic tumor models. Anti-LAP reduced tumor growth in B16 melanoma (Fig. 1A) and in both intracranial (orthotopic) (Fig. 1, B to E, and fig. S1A) and subcutaneous (Fig. 1, F and G) glioblastoma (GBM) (GL261) models. Anti-LAP also affected established B16 tumors (fig. S1B). In GBM, an early therapeutic effect was observed because only rare tumor cells were observed at 2 weeks, whereas all control mice developed solid tumors by this time (Fig. 1H and fig. S1C). In CRC, anti-LAP reduced tumor number in the azoxymethane (AOM)/dextran sulfate sodium (DSS) orthotopic model of spontaneously induced CRC (Fig. 1, I and J, and fig. S1, D and E) and in two subcutaneous CRC models, MC38 and CT26 (Fig. 1, K to M). We used The Cancer Genome Atlas (TCGA) data set to study the relationship between the expression of the LAP/TGF-β–encoding gene *TGFB1* and its associated genes (*THBS1*/TSP-1, *LRRC32*/GARP, *HSPA5*/GRP78, and *LTBP1/2*) with cancer patient survival. We found that the relatively high expression of these genes based on *z* score was associated with poorer patient survival (Fig. 1N and fig. S2).

Anti-LAP decreases LAP^+ CD4 T cells and blocks the release of TGF-β

Potential mechanisms of anti-LAP effects include reduction of LAP^+ T cells and/or blocking TGF-β release from the SLC (fig. S3A). Increased numbers of splenic LAP^+ T cells in animals with B16 melanoma were reduced after anti-LAP treatment (Fig. 2A and fig. S3, B and C), as were the frequency of LAP^+ T cells in the tumor and draining lymph nodes (dLNs) (Fig. 2A). Different noncompeting antibodies were used for anti-LAP treatment (clone TW7-28G11) and for measuring LAP^+ cells (clone TW7-16B4) (fig. S3D). To determine whether anti-LAP blocked the release of membrane-bound TGF-β, we used P3U1 cells that overexpress the *Tgfb1* gene and secrete TGF-β when

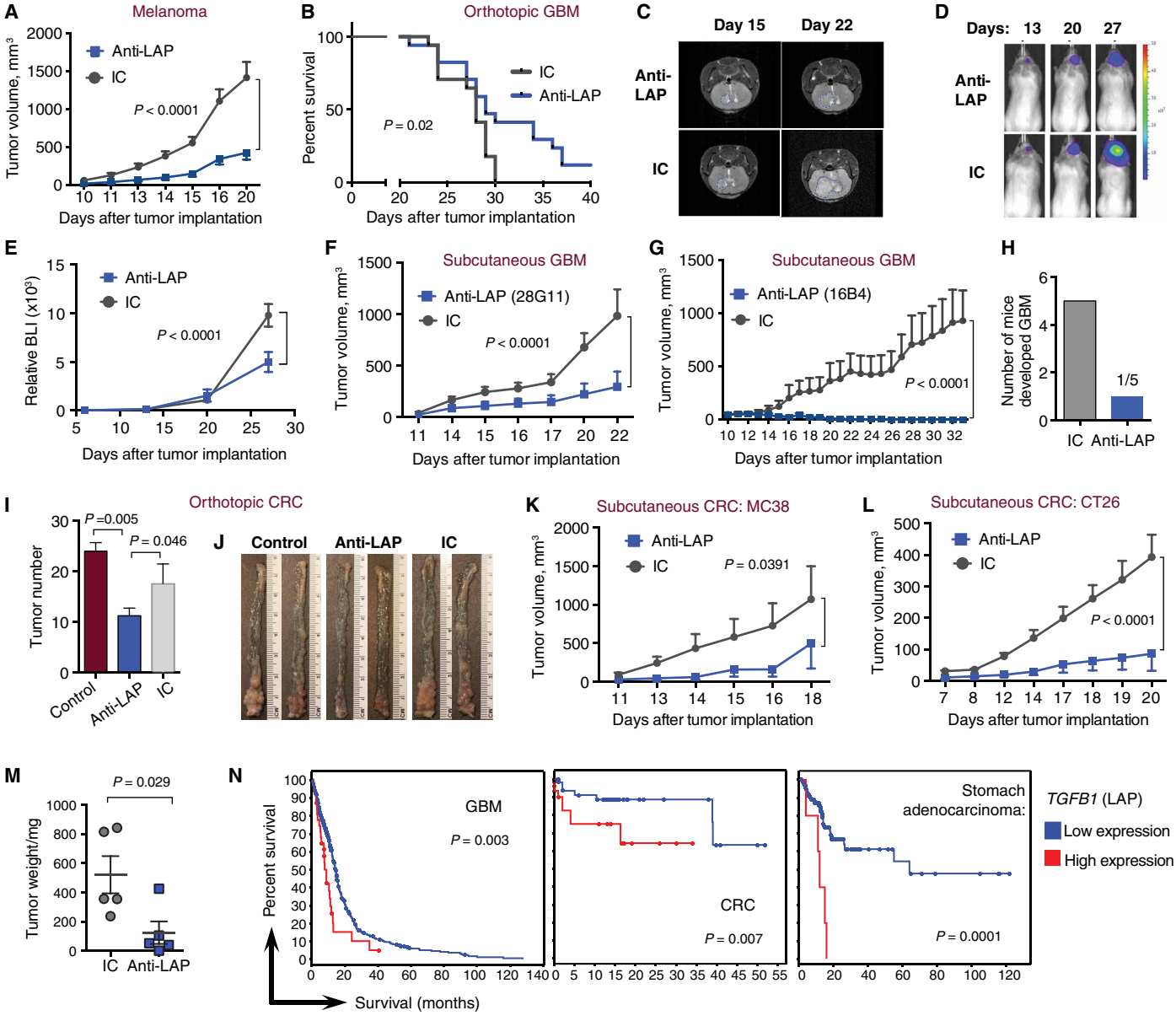

Fig. 1. Therapeutic effect of anti-LAP in cancer models. (**A**) B16 melanoma tumor volume over time in wild-type (WT) mice treated with either anti-LAP (TW7-28G11 clone) or IC antibodies [$n = 6$ (anti-LAP) and $n = 7$ (IC), at the last time point]. Data are representative of at least three independent experiments. (**B**) Survival curves of WT mice with intracranial GL261 GBM treated with anti-LAP clone TW7-16B4 ($n = 17$; data are combined from two independent experiments; log-rank test). Intracranial tumor growth measured by magnetic resonance imaging (representative images) on days 15 and 22 (**C**) and by bioluminescence imaging (BLI; representative images) (**D**) and measured as relative BLI on days 13, 20, and 27 (**E**) [$n = 6$ (anti-LAP) and $n = 7$ (IC), at the last time point]. (**F** and **G**) Tumor volume of subcutaneous GL261 GBM implanted in WT mice and treated with anti-LAP clone TW7-28G11 (F) ($n = 5$) or anti-LAP clone TW7-16B4 (G) ($n = 8$). (**H**) Early therapeutic effect of anti-LAP on intracranial GL261 GBM. Number of mice that developed solid tumors after anti-LAP treatment. (**I** and **J**) Orthotopic AOM/DSS induced CRC in WT mice treated with anti-LAP; tumor number (I) and representative images (J) of CRC colons [$n = 9$ (anti-LAP and IC) and $n = 5$ (control); one-way ANOVA]. Data are representative of two independent experiments. (**K** and **L**) Tumor volume of subcutaneous MC38 (K) ($n = 5$) and CT26 (L) ($n = 5$) CRC models in WT mice treated with anti-LAP. Data are representative of two independent experiments. (**M**) CT26 tumor weight measured at day 20 ($n = 5$; two-tailed t test). (**N**) Percent survival in patients with relatively high or low mRNA expression of *TGFB1* (LAP) based on z score. The "high" expression group was determined on the basis of precomputed z score value from gene expression (greater than 0.005 to 0.5), whereas the "low" group consisted of the remaining patients in the data set. Graphs and P values were downloaded from TCGA data set via cBioPortal (*49*, *50*). Error bars, means ± SEM. Two-way ANOVA (A, E to G, K, and L) was used for P value calculations. P values for the last time points are shown.

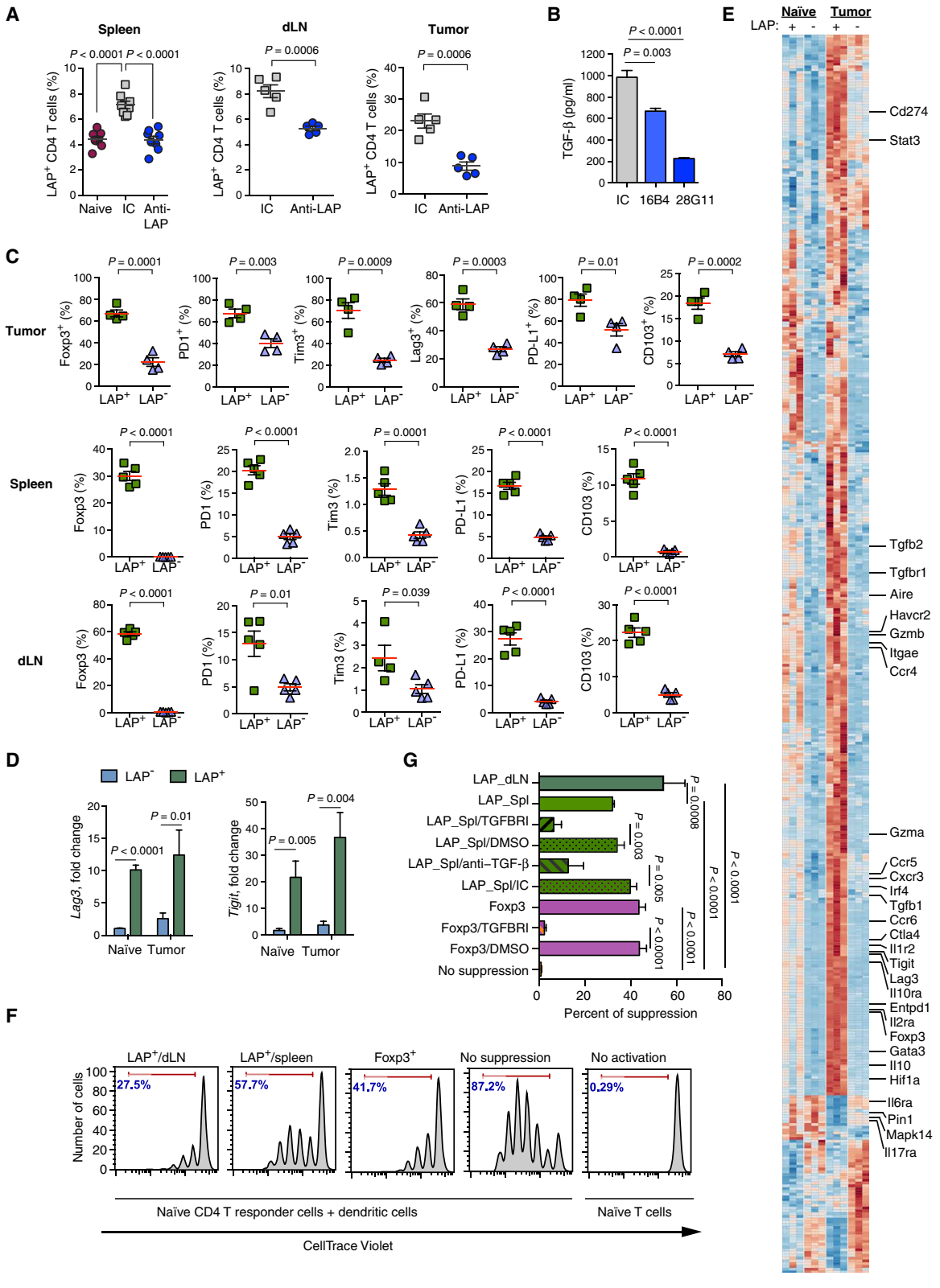

Fig. 2. Modulation of LAP$^+$ CD4 T cells after anti-LAP treatment. (**A**) Frequency of LAP$^+$ T cells in naïve and anti-LAP– or IC-treated B16 melanoma–bearing mice. Mice were treated with anti-LAP clone TW7-28G11 and LAP$^+$ T cells measured with a noncompeting anti-LAP clone (TW7-16B4) by flow cytometry in the spleen (n = 8), dLN, and tumor (n = 5). Data are from at least three independent experiments. (**B**) Active TGF-β release from P3U1 cells expressing mouse LAP/TGF-β treated with anti-LAP clones TW7-16B4 and TW7-28G11 or IC, measured by enzyme-linked immunosorbent assay (n = 3); for more details, see Materials and Methods. Representative of three independent experiments. (**C**) Expression of indicated immune markers in LAP$^+$ versus LAP$^-$ T cells in the spleen, dLN, and tumor of B16 melanoma–bearing mice by flow cytometry (n = 5); representative of two independent experiments. (**D**) Quantitative reverse transcription PCR (qRT-PCR) analysis of *Lag3* and *Tigit* in LAP$^+$ and LAP$^-$ T cells isolated from naïve or B16 tumor–bearing mice (n = 3). (**E**) Heat map of differentially expressed genes in LAP$^+$ and LAP$^-$ T cells isolated from naïve or B16 tumor–bearing mice ordered by Euclidian distance–based hierarchical clustering (n = 3). (**F** and **G**) In vitro suppression of naïve CD4$^+$ T cell proliferation by LAP$^+$ T cells sorted from spleens and dLNs of melanoma-bearing mice. Representative histograms of proliferation of responder CD4$^+$ T cells (F) and percent suppression (G) are shown. Foxp3$^+$ cells served as controls. Indicated samples were treated with TGF-β receptor inhibitor (TGFBRI), dimethyl sulfoxide (DMSO) control, anti–TGF-β or IC antibody (n = 4 to 11; combined data from four experiments, normalized to the level of suppression of LAP$^+$ cells in the spleen). Error bars, means ± SEM. One-way ANOVA [A (left), B, and G] and two-tailed t test [A (middle and right), C, and D] were used for P value calculations.

LAP is activated. Both 16B4 and 28G11 anti-LAP clones reduced the release of TGF-β (Fig. 2B). Thus, anti-LAP decreases LAP^+ cells and blocks TGF-β release from the cell.

LAP^+ CD4 T cells from tumor-bearing mice have suppressive properties

We measured markers associated with T_{regs} (Foxp3), exhausted T cells (Lag3, PD1, PD-L1, and Tim3), and CD103 in TILs from B16 melanoma mice on both LAP^+ and LAP^- T cells. Expression of these markers was increased on LAP^+ versus LAP^- T cells (Fig. 2C and fig. S3E). A similar tolerogenic phenotype was observed for LAP^+ T_{regs} from the dLNs and spleens of tumor-bearing mice (Fig. 2C and fig. S3, F and G). We also measured gene expression and found that cancer-associated genes, including *Lag3*, *Tigit*, and *Vcam*, were expressed at higher levels in LAP^+ versus LAP^- T cells (Fig. 2D and fig. S4A). *Irf4*, which has been shown to promote effector function of T_{regs} (*16*), was also overexpressed in LAP^+ T cells (fig. S4A). Using the NanoString PanCancer Immunology code set, we found 480 genes differentially expressed between B16 melanoma and control mice (Fig. 2E). Among them, genes associated with effector T_{reg} function, such as *Aire*, *Gata3*, *Irf4*, *Foxp3*, *Stat3*, *Tgfb1*, *Tgfb2*, *Entpd1* (CD39), *Itgae* (CD103), *Il10*, *Gzma*, and *Gzmb*, and cancer-associated T cell markers, such as *Havcr2* (Tim3), *Ctla4*, *Tigit*, and *Lag3*, were expressed at a higher level in LAP^+ T cells in naïve mice. These genes were further up-regulated in LAP^+ T cells in tumor-bearing mice (Fig. 2E). On the other hand, genes associated with T cell activation, including *Il6ra*, *Pin1*, and *Mapk14*, were down-regulated in LAP^+ T cells in tumor-bearing mice (Fig. 2E).

Because Foxp3 is a marker of T_{regs} in mice, we analyzed the relationship between LAP and Foxp3 in B16 tumor–bearing mice. We performed principal components analysis (PCA) on the NanoString-based gene expression data in LAP^+/LAP^-/$Foxp3^+$/ $Foxp3^-$ CD4 T cell subsets. We found that PC1 was associated with the variance between $Foxp3^+$ and $Foxp3^-$ generated data sets, whereas PC2 was associated with the variance between LAP^+ and LAP^- generated data sets. Thus, in addition to the differences between $Foxp3^+$ and $Foxp3^-$, we found that LAP^+ T cell subsets clustered differently from LAP^- T cells in both T_{reg} and non-T_{reg} CD4 populations (fig. S4B). We analyzed the distribution of LAP^+/LAP^-/$Foxp3^+$/$Foxp3^-$ T cell subsets in vivo and found that most LAP^+ T cells were $Foxp3^+$ both in the periphery and in the tumor (fig. S4C). LAP^+ T cells from both dLNs and spleens of tumor-bearing mice reduced the proliferation of responder $CD4^+$ T cells in vitro (Fig. 2, F and G). Blocking TGF-β signaling with either a TGF-β receptor inhibitor or an anti–TGF-β mAb (Fig. 2G) reduced suppression, indicating that LAP^+ T cells suppressed T cell proliferation in vitro through a TGF-β–dependent mechanism.

Anti-LAP treatment modulates dendritic cell subsets in the spleen

Antigen-presenting cells play a key role in antitumor immunity. Because anti-LAP blocks the secretion of TGF-β, which is known to interfere with the maturation of splenic antigen-presenting cells (*17*), we investigated anti-LAP on dendritic cells (DCs) in the spleen in the B16 melanoma model. We measured CD11c-Hi/CD11b-Int (subsequently referred to as CD11c-Hi) and CD11c-Int/CD11b-Hi (CD11c-Int) cell subsets. CD11c-Hi cells were increased after anti-LAP treatment, whereas CD11c-Int cells were reduced (Fig. 3, A and B). We also measured splenic DCs in the GBM model and observed a similar effect (fig. S5, A and B). In GBM, tumors grow slowly, and the effect of anti-LAP on splenic CD11c/CD11b DCs in GBM was observed with long-term anti-LAP treatment (>3 weeks). CD11c-Int cells express higher levels of LAP versus CD11c-Hi cells (Fig. 3C and fig. S5C), which suggests that CD11c-Int cells are more tolerogenic. Because the function of these two DC subsets is not well defined, we characterized their inflammatory properties. We found that both major histocompatibility complex II (MHCII) and CD86 were expressed at higher levels in CD11c-Hi versus CD11c-Int cells (Fig. 3D and fig. S5D). We then sorted these two DC subsets, stimulated them with lipopolysaccharide (LPS) or anti-CD40, and measured cytokine expression. We found that *Il10* was expressed at higher levels and *Il12* was expressed at lower levels in the CD11c-Int subset (Fig. 3E), indicating a more tolerogenic phenotype as compared with CD11c-Hi cells. To determine whether these DC subsets affected CD8 T cells, we cocultured them with labeled $CD8^+$ naïve T cells and measured cytokine secretion and growth. We found increased expression of interferon-γ (IFN-γ) and tumor necrosis factor–α (TNF-α) in cells cocultured with the CD11c-Hi subset (Fig. 3F), demonstrating that CD11c-Hi cells promote an effector phenotype in $CD8^+$ cells. Furthermore, CD11c-Hi cells supported $CD8^+$ T cell survival to a greater extent than the CD11c-Int subset (Fig. 3G and fig. S5E). Last, we found that anti-LAP treatment decreased LAP^+ CD11c-Int cells (Fig. 3H and fig. S5F) and reduced the expression of the tolerance-associated proteins PD-L1 and CD103 in CD11c-Int cells (Fig. 3I and fig. S5G). This is presumably secondary to the reduction of TGF-β by anti-LAP (Fig. 2B) because both genes could be up-regulated by TGF-β (*18*, *19*). Thus, anti-LAP increased DCs with a proinflammatory phenotype and decreased DCs with an anti-inflammatory phenotype in the spleen. We found that membrane LAP expression was reduced in $CD11c^+$ cells in the spleen, dLN, and tumor after anti-LAP treatment (Fig. 3J and fig. S5H), indicating that anti-LAP may also affect DCs in the tumor microenvironment. We did not identify CD11c/CD11b subsets in the dLN or tumor (fig. S5I).

Anti-LAP treatment enhances antitumor adaptive immune responses

To test whether $CD8^+$ T cells were required for the therapeutic effect of anti-LAP, we implanted B16 melanoma in CD8-deficient mice and found that the therapeutic effect of anti-LAP was abolished (Fig. 4A). Consistent with this, the therapeutic effect of anti-LAP was also reversed in animals treated with anti-CD8 (fig. S6A). No difference was observed in CD4-deficient mice (fig. S6B). When we analyzed TILs from mice implanted with B16 melanoma, we found an increase in infiltrating $CD8^+$ T cells after anti-LAP treatment, whereas $CD4^+$ T cells did not change (Fig. 4B and fig. S6C). Similar results were observed in the intracranial GBM model (fig. S6D). Intratumoral $CD8^+$ T cells expressed higher levels of the proliferation marker Ki67, the proinflammatory cytokine IFN-γ, and the degranulation marker CD107 (Fig. 4B and fig. S6E). Anti-LAP treatment also increased the ratio of $CD8^+$ T cells to $Foxp3^+$ T_{regs} in the tumor in both B16 melanoma and intracranial GL261 GBM models (Fig. 4B and fig. S6, E and F). We then examined the dLNs and spleens of B16 melanoma–bearing mice. In dLN, anti-LAP enhanced the proliferation of $CD8^+$ T cells, increased the levels of TNF-α in $CD8^+$ and $CD4^+$ T lymphocytes, and increased natural killer (NK) cells and the levels of granzyme B they express (Fig. 4C and fig. S6G). In the spleen, we observed higher levels of granzyme B, CD107, and ICOS (inducible T cell costimulator) in $CD8^+$ T cells after anti-LAP treatment, demonstrating a stronger effector phenotype of cytotoxic T cells after treatment. In addition, the frequency of NK cells and the expression of granzyme B by NK cells were increased. Furthermore, the CD44 activation marker was up-regulated

in CD4$^+$ T cells (Fig. 4D and fig. S6H). The percentage of LAP$^+$ CD8 T cells was very low in the spleen, dLN, and tumor and did not change with anti-LAP treatment (fig. S6, I and J), suggesting that these cells do not play a substantial role in the antitumor effect of anti-LAP. Together, these results demonstrate that anti-LAP affects adaptive immune responses both systemically and within the tumor, driving them to a more inflammatory phenotype.

Anti-LAP treatment affects tolerogenic CD103$^+$ CD8 T cells

We consistently found a reduction of CD103$^+$ CD8 T cells in both spleens and dLNs after anti-LAP treatment (Fig. 5A). TGF-β plays an important role in the induction of CD103$^+$ CD8 T cells (*20*), which may explain why anti-LAP reduces their number. Because the frequency of infiltrating CD103$^+$ CD8 T cells in B16 tumors was very low (fig. S7, A and B), we focused on CD103$^+$ CD8 T cells in the periphery. We measured gene expression in CD103$^+$ and CD103$^-$ CD8 T cells from the dLNs and spleens of naïve and B16 melanoma–bearing mice using the NanoString PanCancer Immunology code set. We found 171 differentially expressed genes between groups (Fig. 5B), among them, activation and effector markers, including *Cd44*, *Gzma*, *Gzmm*, *Gzmk*, *Il2rb*, *Prdm1*, *Il18r1*, *Tbx21*, *Eomes*, and *Ccr2*; these genes were specifically overexpressed in CD103$^-$ CD8 T cells in naïve mice and were further

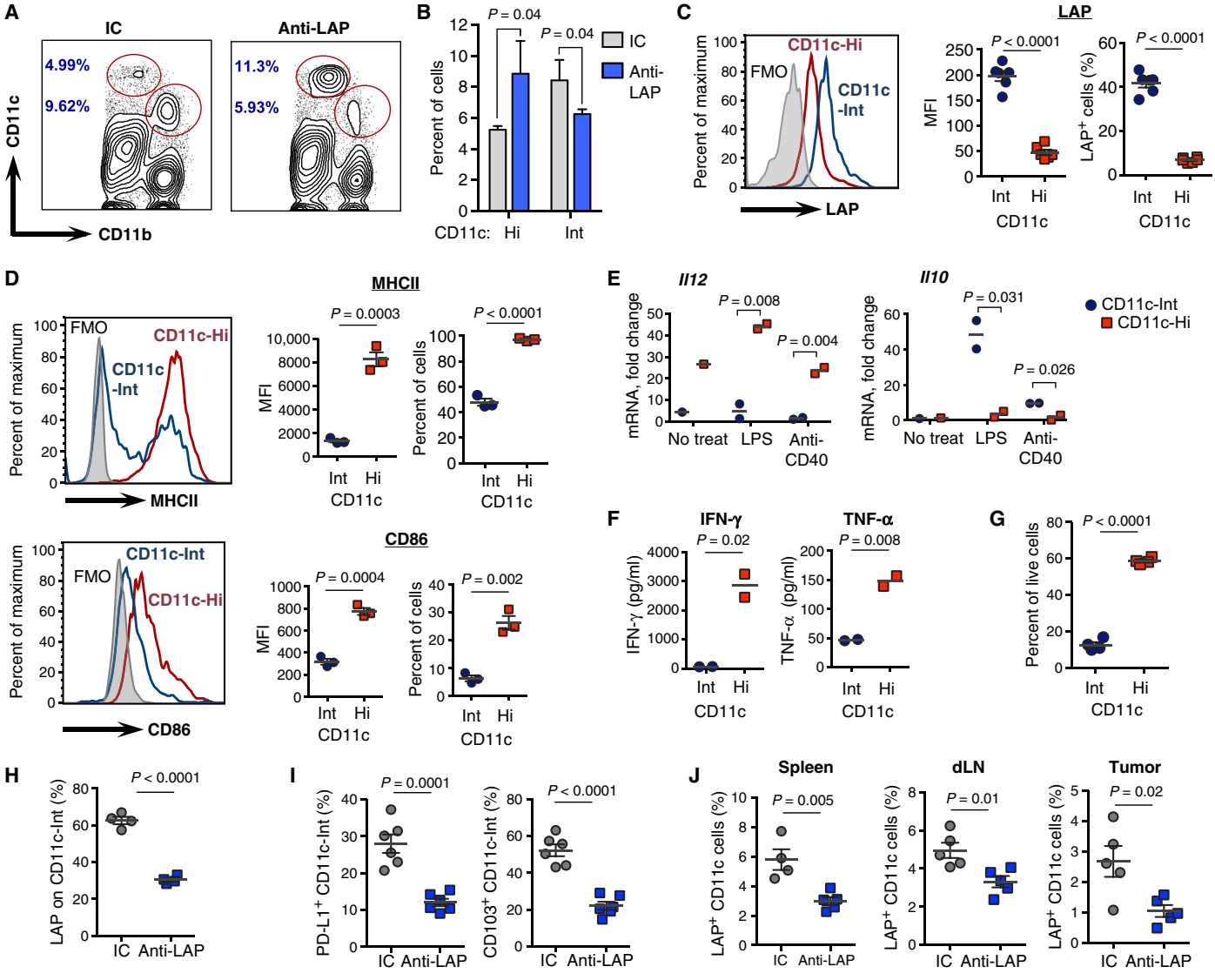

Fig. 3. Modulation of DC subsets after anti-LAP treatment. (**A** and **B**) Effect of anti-LAP treatment on CD11c-Hi/CD11b-Int and CD11c-Int/CD11b-Hi DCs on the spleen, shown as contour dot plots (A) and quantified as cell frequencies (B) (n = 3; representative of two independent experiments). (**C**) Expression of LAP on CD11c-Hi and CD11c-Int DCs. Fluorescence minus one (FMO) control was used as a negative control for staining (n = 6; representative of two experiments). (**D**) Expression of MHCII and CD86 on CD11c-Hi and CD11c-Int DCs (n = 3; representative of two experiments). MFI, mean fluorescence intensity. (**E**) *Il12* and *Il10* expression measured by qRT-PCR after stimulation of CD11c-Int and CD11c-Hi cells sorted from the spleen and treated with LPS or anti-CD40. (**F** and **G**) CD8$^+$ T cells were cocultured with CD11c-Int or CD11c-Hi for 3 days, and IFN-γ and TNF-α were measured in the supernatants (F) and live CD8$^+$ T cells (G) quantified by flow cytometry (n = 4; representative of three experiments). (**H** and **I**) Expression of LAP (H) (n = 4), PD-L1, and CD103 (I) (n = 6) in splenic CD11c-Int cells from tumor-bearing mice after anti-LAP treatment; representative of three experiments. (**J**) Expression of LAP in CD11c$^+$ cells from the spleen, dLN, and tumor of B16 tumor–bearing mice after anti-LAP treatment (n = 4 to 5; data are from two independent experiments). Error bars, means ± SEM. Two-tailed t test was used for P value calculations.

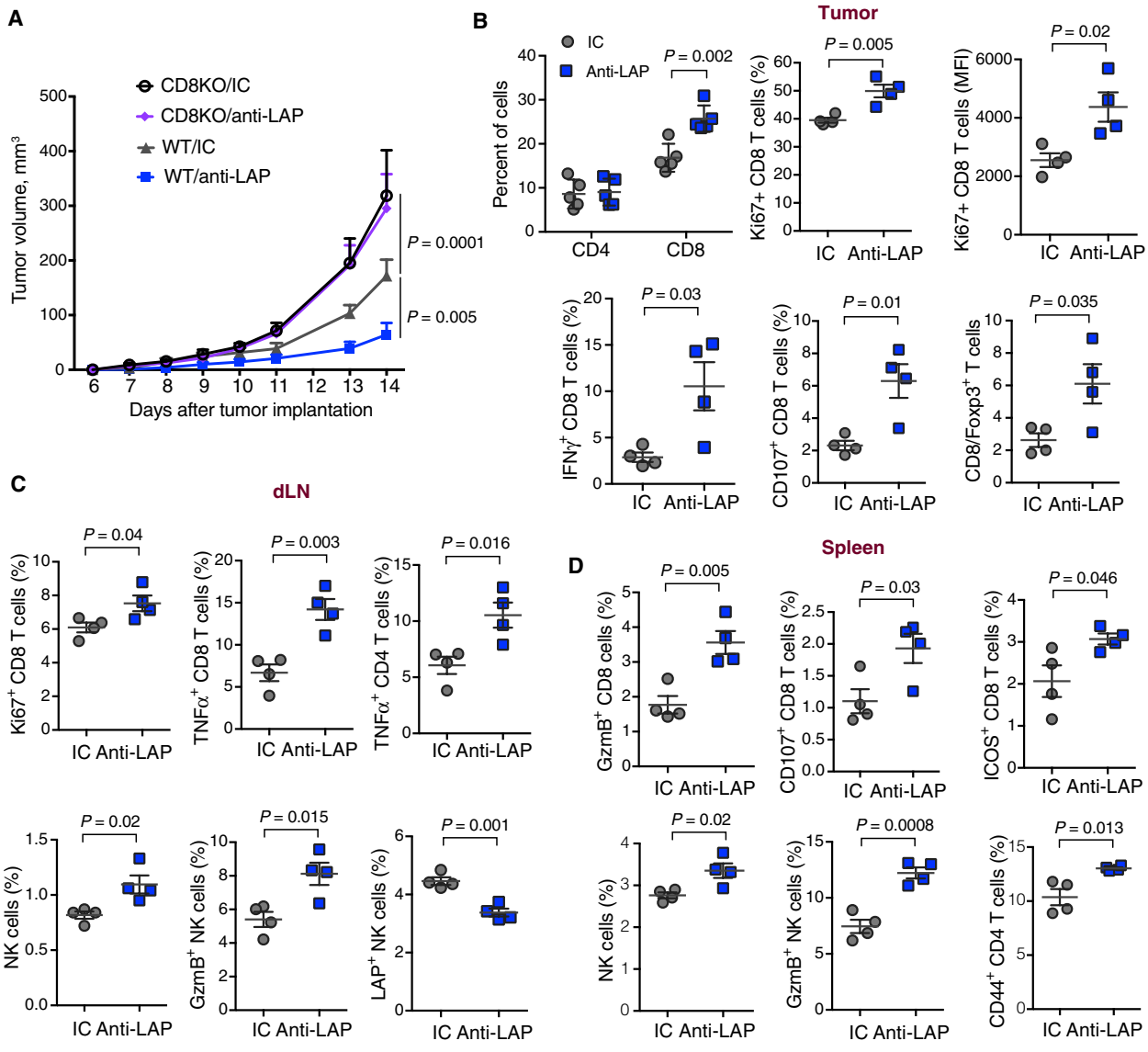

Fig. 4. Effect of anti-LAP treatment on the adaptive immune response. (**A**) Tumor volume measured over time in WT and CD8KO mice implanted with B16 melanoma cells and treated with either anti-LAP or IC antibodies [$n = 5$ (CD8KO/anti-LAP and WT/anti-LAP) and $n = 4$ (CD8KO/IC and WT/IC)]. Data are representative of two independent experiments. (**B** to **D**) Analysis of the immune response in the tumor (B), dLN (C), and spleen (D) of B16 tumor–bearing mice by flow cytometry ($n = 4$). Data are representative of two independent experiments. Error bars, means ± SEM. Two-way ANOVA (A) and two-tailed *t* test (B to D) were used for *P* value calculations. *P* values for the last time point are shown.

up-regulated in tumor-bearing mice. On the other hand, negative regulators of T cell activation, including *Egr3*, *Ctla4*, and *Tgfbr2*, were higher in CD103$^+$ CD8 T cells. The T_{reg}-associated genes *Il2ra*, *Foxp3*, and *Rorc* (*21*–*23*) were up-regulated in CD103$^+$ CD8 T cells in tumor-bearing mice. Tumor suppressor genes, such as *Erg1* and *Rrad*, were down-regulated in CD103$^+$ cells from tumor-bearing mice versus naïve mice, whereas oncogenes, such as Plaur and Vcam, were up-regulated, suggesting that the tumor itself may further modulate the CD103$^+$ T cell subset. In the intracranial GBM model, CD103$^+$ CD8 T cells infiltrate the tumor, and anti-LAP reduced these cells both systemically and in the tumor (fig. S7C).

To further investigate CD103$^+$ and CD103$^-$ CD8 T cell subsets under naïve versus tumor conditions, we performed PCA on the global gene signature and found differential clustering of CD103$^+$ versus CD103$^-$ CD8 T cell subsets under both naïve and tumor conditions (Fig. 5C). PC1 mainly accounts for the variance between CD103$^+$ and CD103$^-$ generated data sets, whereas PC2 accounts for the variance between tumor and naïve generated data sets. Thus, CD103$^+$ marks a CD8 T cell population that is different both in naïve mice and under tumor conditions. We then measured protein expression of activation markers IFN-γ, TNF-α, GzmA, CD44, Eomes, interleukin-18 receptor (IL-18R), IL-2RB, IL-2, CD107, and Ly6C on CD103$^+$ versus CD103$^-$ CD8 T cells in the spleens and dLNs of melanoma-bearing mice. We found that CD103$^+$ CD8 cells expressed lower levels of these markers (Fig. 5D and fig. S7, D and E). KLRG1 was also decreased in CD103$^+$ CD8 T cells. On the other hand, IL-10, CTLA4, and CD25/IL-2RA were up-regulated in CD103$^+$ CD8 T cells from dLNs, consistent with the regulatory phenotype of CD103$^+$ CD8 T cells. We then found that CD103$^+$ CD8 T cells

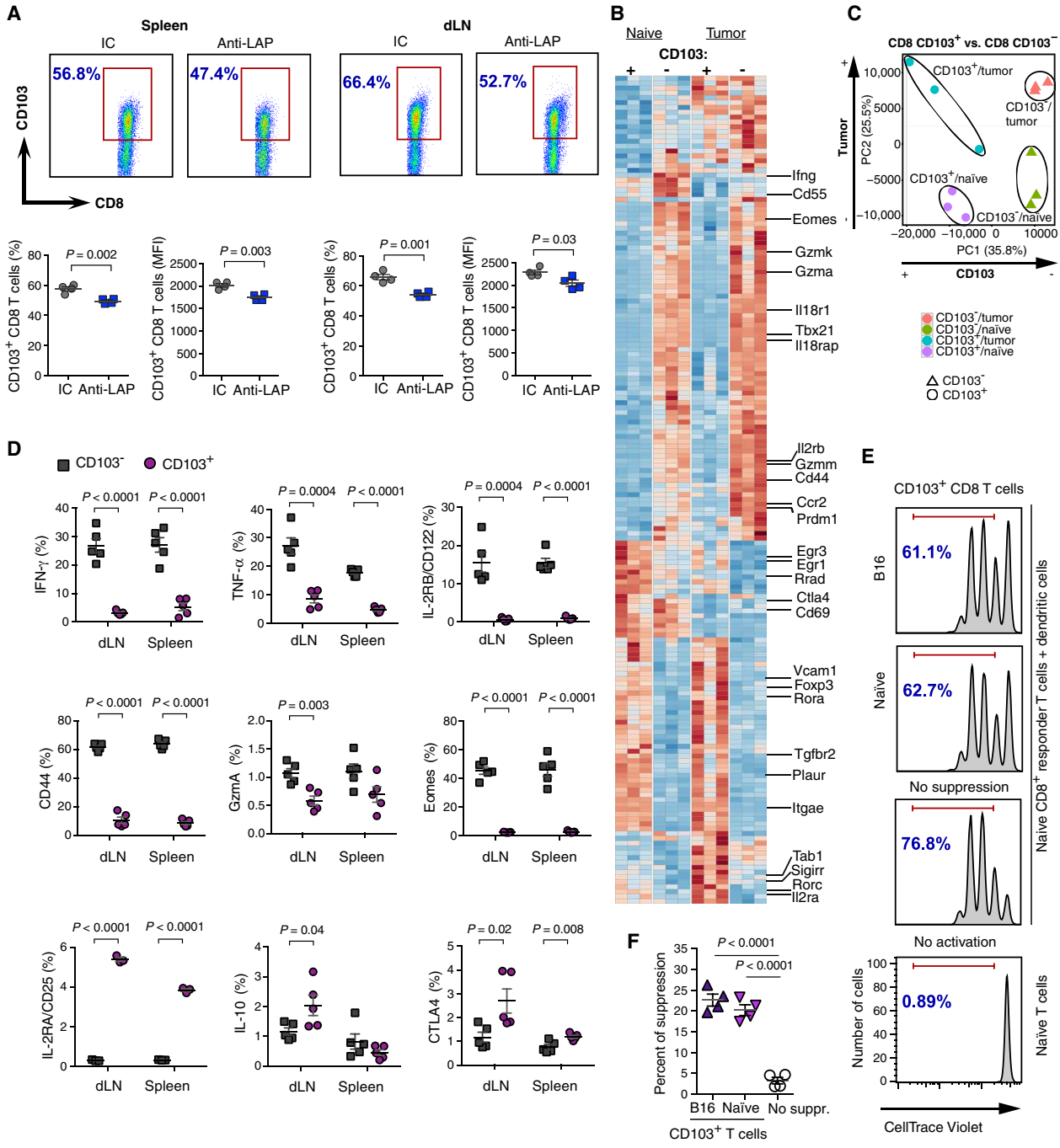

Fig. 5. CD103$^+$ CD8 T cells are decreased by anti-LAP and have regulatory properties. (**A**) CD103$^+$ CD8 T cells after anti-LAP treatment in spleens and dLNs by flow cytometry. Dot plot graphs (top) and statistical calculations (bottom) for cell frequencies and MFI are shown ($n = 4$). Data are representative of at least three independent experiments. (**B**) Heat map showing differentially expressed genes in CD103$^+$ and CD103$^-$ CD8 T cells from either naïve or B16 tumor–bearing mice ($n = 3$). (**C**) PCA of the global gene expression profiles shown in (B). (**D**) Phenotypic characterization of CD103$^+$ and CD103$^-$ CD8 T cells in dLNs and spleens of B16 melanoma–bearing mice by flow cytometry ($n = 3$ to 5; data are combined from two independent experiments). (**E** and **F**) In vitro suppression of naïve CD8$^+$ T cell proliferation by CD103$^+$ CD8 T cells isolated from naïve or melanoma-bearing mice. (E) Representative histograms of proliferation of responder CD8$^+$ T cells and (F) percent of suppression ($n = 4$; data are representative of three independent experiments). Error bars, means ± SEM. Two-tailed *t* test (A and D) and one-way ANOVA (F) were used for *P* value calculations.

isolated from either B16 melanoma–bearing or naïve mice suppressed CD8$^+$ T cell proliferation (Fig. 5, E and F). Suppression was mediated by the PD1/PD-L1 axis because it was blocked by anti-PD1 or anti–PD-L1 antibodies (fig. S7F). Consistent with this, CD103$^+$ CD8 T cells expressed a higher level of PD-L1 than CD103$^-$ CD8 T cells (fig. S7, G and H). Anti-PD1 and anti-LAP antibodies had comparable effects on B16 tumor growth (fig. S7I). We then examined the in vivo tumor-promoting role of CD103$^+$ CD8 T cells by adoptively transferring CD103$^+$ or CD103$^-$ CD8 T cells from B16 melanoma–bearing mice to CD8-deficient animals. We found greater tumor growth in

animals that received CD103$^+$ CD8 T cells and smaller tumor growth in animals that received CD103$^-$ CD8 T cells (Fig. 6A and fig. S8A). Co-transfer of CD103$^+$/CD103$^-$ CD8 T cells increased tumor growth compared with the transfer of CD103$^-$ CD8 T cells alone. Without T cell transfer [phosphate-buffered saline (PBS) group], there was greater tumor growth compared with all the CD8$^+$ T cell transfer groups, demonstrating that CD8$^+$ T cells control tumor growth. The increased tumor growth that we observed in the PBS group as compared with the CD103$^+$ CD8 T cell group could be explained by the stability of CD103$^+$ CD8 T cells after adoptive transfer: Only 40% of cells remain CD103$^+$ CD8 T cells (Fig. 6B).

We isolated these cells at the end of the experiment and found that they maintained expression of CD103 and lower levels of proinflammatory genes (Fig. 6B and fig. S8B). We observed a similar effect when CD103$^+$ or CD103$^-$ CD8 T cells were adoptively transferred from untreated mice (fig. S8C). To further investigate the role of CD103, we treated B16 melanoma– and MC38 CRC–bearing mice with anti-CD103 antibody, which primarily targets CD103$^+$ CD8 T cells (fig. S8D). We

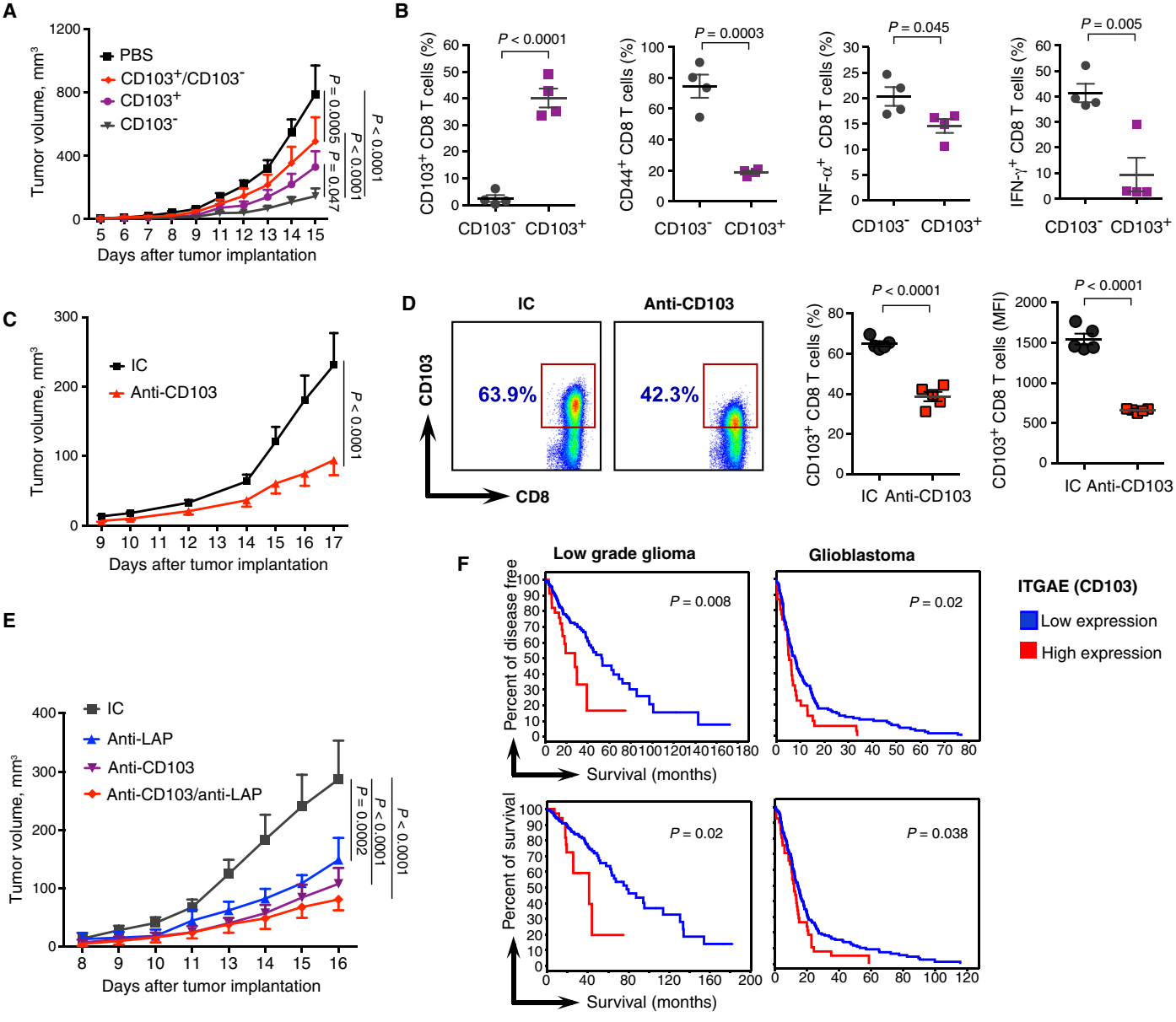

Fig. 6. CD103$^+$ CD8 T cells have protumorigenic properties. (**A**) B16 melanoma tumor volumes in mice adoptively transferred with PBS ($n = 4$), CD103$^+$ ($n = 5$), CD103$^-$ ($n = 4$), or CD103$^+$/CD103$^-$ ($n = 4$) CD8 T cells from B16 melanoma mice to CD8KO mice. Data are representative of two independent experiments. (**B**) Expression of CD103, CD44, TNF-α, and IFN-γ in mice after adoptive transfer of CD103$^+$ CD8 T cells, as compared with CD103$^-$ CD8 T cells by flow cytometry ($n = 4$). (**C**) Tumor volumes measured over time in the B16 melanoma model treated with anti-CD103 (clone M290; $n = 10$). (**D**) Expression of CD103 on CD8 cells in dLNs of mice from (C) by flow cytometry with a noncompeting 2E7 clone of anti-CD103. Both frequency of CD103$^+$ CD8 T cells and MFI are presented ($n = 5$). (**E**) Tumor volumes measured over time in the B16 melanoma model treated with IC, anti-CD103, anti-LAP, or combined anti-CD103/anti-LAP ($n = 5$). (**F**) Percent survival in patients with relatively high or low mRNA expression of *ITGAE* (CD103) based on *z* score (details are as in Fig.1N). Results for low-grade glioma and GBM are shown. Error bars, means ± SEM. Two-way ANOVA (A, C, and E) and two-tailed *t* test (B and D) were used for *P* value calculations. *P* values for the last time points are shown.

found that anti-CD103 treatment reduced tumor growth (Fig. 6C and fig. S8E) and was associated with the reduction of $CD103^+$ CD8 T cells (Fig. 6D). We then asked whether combined targeting of CD103 and LAP would have a synergistic effect; we treated tumor-bearing mice simultaneously with anti-CD103 plus anti-LAP. We did not observe a decrease of B16 tumor growth as compared with single-antibody treatment with either anti-CD103 or anti-LAP (Fig. 6E). Consistent with our findings, in patients with both high- and low-grade gliomas, high CD103 expression was associated with shorter survival (Fig. 6F). CD103 is also expressed in $CD4^+$ T_{regs}, which can contribute to a poorer prognosis. To address the potential role of LAP on $CD103^+$ CD8 T cell function, we examined surface LAP expression and found that the frequency of LAP^+CD103^+ CD8 T cells was very low, and there was no increased LAP expression in $CD103^+$ versus $CD103^-$ CD8 T cells (fig. S8F).

Anti-LAP treatment combined with antigen-specific vaccination enhances tumor immunotherapy and improves immune memory

Because anti-LAP enhances the maturation of antigen-presenting cells, we investigated combining anti-LAP with antigen-specific vaccination. We used B16 melanoma cells that express ovalbumin (B16-OVA) and treatment with DCs loaded with OVA (Fig. 7A). In this model, OVA serves as a tumor-associated antigen. One week after vaccination with OVA-loaded DCs, mice were implanted with B16-OVA and treated with anti-LAP every third day. No mice vaccinated and treated with anti-LAP developed tumors, whereas 60% of mice treated with isotype control (IC) antibody and all mice in the control group developed tumors (Fig. 7B). We then asked whether anti-LAP affected immune memory after DC vaccination. We used a series of markers for the activation and memory of $CD8^+$ T cells, including IL-7R, KLRG1, CCR7, and CD62L. On the basis of previously reported $CD8^+$ T cell memory markers (*24*–*26*), we found an increase of effector memory-like $CD8^+$ T cells in dLNs of anti-LAP–treated mice (Fig. 7, C to G, and fig. S9A). Consistent with our results above, $IL\text{-}7R^+CD103^-$ CD8 T cells were increased in mice treated with anti-LAP (Fig. 7H and fig. S9B).

We also investigated the intracranial GBM model in which glioma cells expressing OVA (GL261-OVA) were implanted (Fig. 7I). One week after vaccination with OVA-loaded DCs, mice were implanted with GL261-OVA and treated with anti-LAP. Disease onset was delayed, and on the basis of magnetic resonance imaging (MRI), none of the anti-LAP–treated mice developed tumors (Fig. 7, J and K). On day 114, we rechallenged mice that did not develop tumors by subcutaneously implanting GL261-OVA and followed them for an additional month. None of these mice developed tumors, indicating that they had developed antigen-specific immunity against the tumor. We investigated the immune response against OVA in surviving mice and found that anti-LAP–treated mice developed increased numbers of both OVA-specific CD8 cells (Fig. 7L) and memory cells, as measured by IL-7R and CD62L markers (Fig. 7, M and N). To investigate the contribution of anti-LAP to immune memory, we vaccinated mice with DCs loaded with OVA and treated them with anti-LAP for 4 weeks (Fig. 7O). One month later, we rechallenged the mice with a small number of subcutaneously injected GL261-OVA cells. Two months later, we analyzed $CD8^+$ T cells and found specific up-regulation of $IL\text{-}7R^+CD44^+$ CD8 T cells in anti-LAP–treated mice (Fig. 7P and fig. S9C), indicating that anti-LAP supports antitumor memory. Thus, combination therapy with anti-LAP improved the immune response to antigen-specific DC vaccination and enhanced immune memory.

DISCUSSION

Although targeting T_{regs} is an important avenue to boost tumor immunity, this approach has been limited because of a lack of druggable T_{reg} targets and a lack of specificity for T_{regs} (*27*, *28*). We found that targeting LAP may be an effective way to affect T_{regs} and boost tumor immunity because the LAP/TGF-β complex identifies a subset of highly suppressive T_{regs} that are up-regulated in human malignancies (*7*, *8*, *29*). Consistent with multiple roles of TGF-β, we found increased cytotoxic T lymphocyte (CTL) responses, reduction of tolerogenic $CD103^+$ CD8 T cells, activation of NK cells, maturation of DCs, and improved immune memory after anti-LAP treatment. In humans, LAP^+Foxp3^+ T cells are more suppressive than LAP^-Foxp3^+ T cells (*7*). Consistent with this, anti-LAP did not affect $Foxp3^+$ T cell numbers in our studies. Foxp3 can also be transiently expressed in activated effector T cells in humans (*30*), and the accumulation of a Foxp3-lo population, represented by non-T_{regs}, correlates with better survival of CRC patients than Foxp3-hi cells (*31*). These studies may explain the different roles of T_{regs} in CRC reported by investigators.

We found that $CD103^+$ CD8 T cells have a tolerogenic immune profile, exhibit suppressive properties, and have a tumor-promoting role in vivo as compared with $CD103^-$ CD8 T cells. Anti-LAP treatment reduced $CD103^+$ CD8 T cells, presumably because it decreases bioavailable TGF-β, which regulates the generation of $CD103^+$ CD8 T cells (*19*, *32*, *33*). TGF-β has been demonstrated to regulate the generation of $CD103^+$ CD8 T cells (*19*, *32*, *33*). Furthermore, we found that direct targeting of CD103 by an anti-CD103 antibody that reduces $CD103^+$ CD8 T cells in mice similar to what we observed with anti-LAP also had a therapeutic effect in the B16 melanoma and MC38 CRC models. Anti-CD103 antibody appears to act systemically in the B16 melanoma model because only a few $CD103^+$ CD8 T cells infiltrate the tumor in this model. Combinatorial treatment with anti-LAP and anti-CD103 did not result in a synergistic therapeutic effect, indicating that the LAP and CD103 pathways overlap. A previous study of anti-CD103 did not show a therapeutic effect in the CT26 model of CRC (*34*). Different roles for $CD103^+$ CD8 T cells have been reported. Some studies report increased effector function against cancer cells (*20*, *32*, *35*, *36*), whereas others demonstrate that $CD103^+$ CD8 T cells could be regulatory in transplantation models and autoimmunity (*37*–*41*). Our study supports these latter observations and extends them to cancer. It is possible that $CD103^+$ CD8 T cells kill cancer cells in the tumor environment while systemically suppressing T cell growth. CD103 has been described as a marker of $CD4^+$ regulatory cells and is present in tolerogenic DCs (*2*, *34*, *42*–*44*).

LAP is expressed not only in $CD4^+$ T cells but also in CD8 cells, γδ T cells, NK cells, B cells, and DCs (*45*–*48*). Thus, the antitumor effect of anti-LAP could be related to multiple targets. DCs play a key role in tumor antigen-specific vaccination, and we found that anti-LAP plus DC vaccination enhanced the antitumor effects of DC vaccination. Immature DCs express higher levels of LAP, and we found that LAP^+ DCs in humans have suppressive properties (*45*).

Although we demonstrate the therapeutic efficacy of anti-LAP antibody in a range of models, the models do not always predict responses in humans. Furthermore, the subcutaneous models we studied do not mimic the natural tumor environment in humans. Nonetheless, LAP^+ cells are increased in human cancer, have a tolerogenic function, and predict poor prognosis in human cancer (*7*, *8*, *29*). Thus, despite the limitations of animal models, targeting LAP^+ cells is consistent with the importance of TGF-β and T_{regs} in the physiology of cancer in humans.

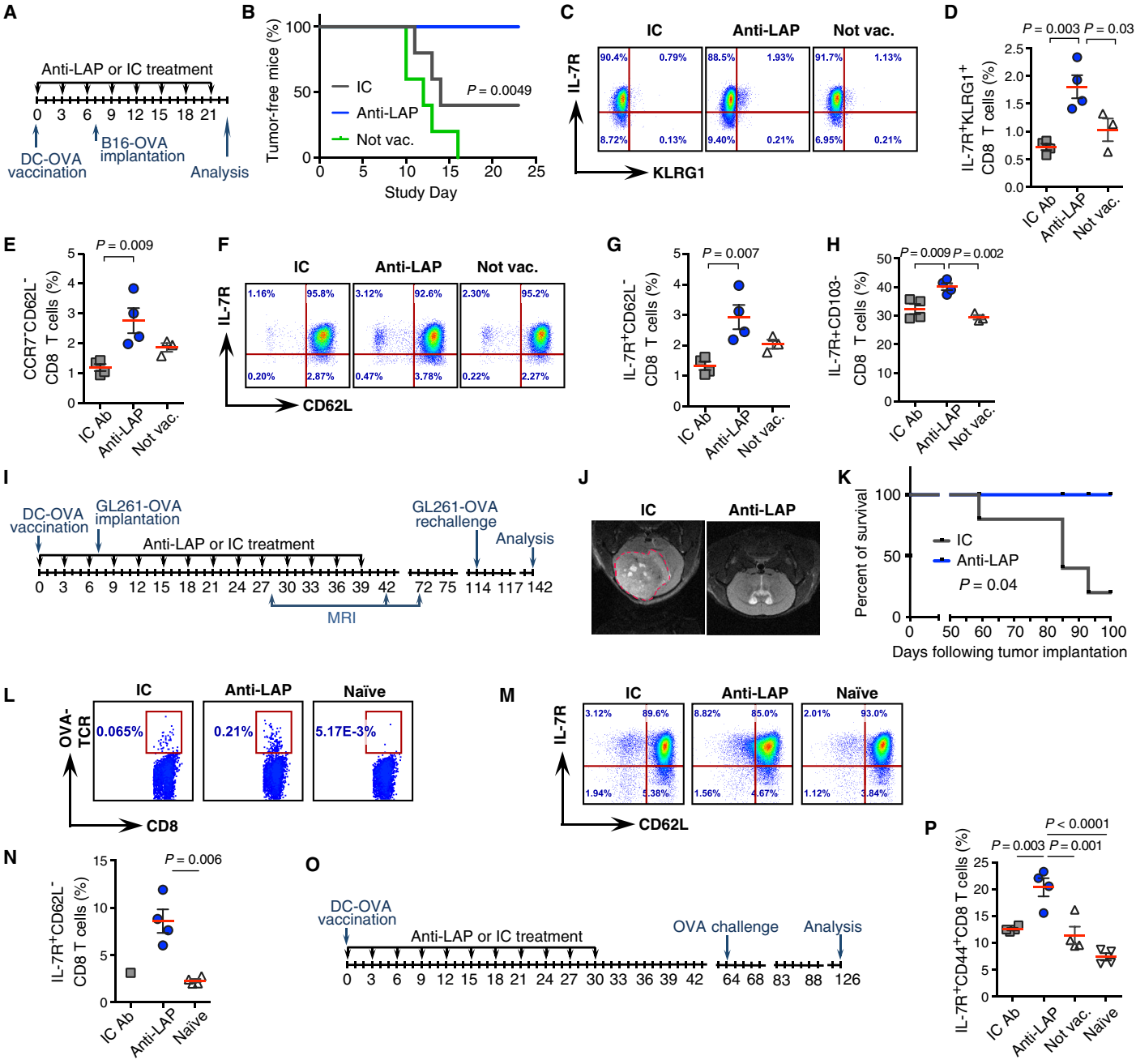

Fig. 7. Anti-LAP treatment combined with antigen-specific vaccination enhances tumor immunotherapy and improves immune memory. (**A**) Study design. (**B**) Percentage of tumor-free mice ($n = 5$; log-rank test). Data are representative of two independent experiments. (**C** and **D**) Accumulation of memory-like $CD8^+$ T cells, based on IL-7R and KLRG1 expression in anti-LAP–treated mice. Representative flow cytometry dot plots (C) and quantification (D) are shown [$n = 4$ (anti-LAP and IC) and $n = 3$ (not vaccinated)]. (**E**) Percentage of memory-like $CD8^+$ T cells, based on CCR7 and CD62L expression in anti-LAP–treated mice [$n = 4$ (anti-LAP and IC) and $n = 3$ (not vaccinated)]. (**F** and **G**) Frequency of memory-like $CD8^+$ T cells, based on IL-7R and CD62L expression in anti-LAP–treated mice. Representative flow cytometry dot plots (F) and quantification (G) are shown [$n = 4$ (anti-LAP and IC) and $n = 3$ (not vaccinated)]. (**H**) Percentage of IL-$7R^+CD103^-$ CD8 T cells [$n = 4$ (anti-LAP and IC) and $n = 3$ (not vaccinated)]. (**I**) Study design. (**J**) Representative magnetic resonance images of mice treated with either IC or anti-LAP. (**K**) Survival curves of mice prevaccinated with DC-OVA, implanted with intracranial GBM, and treated with anti-LAP ($n = 5$; log-rank test). (**L**) Frequencies of OVA-TCR–specific $CD8^+$ T cells (stained with H-2Kb OVA Pentamer) in mice treated with anti-LAP. (**M** and **N**) Accumulation of memory-like $CD8^+$ T cells in anti-LAP–treated mice. Representative flow cytometry dot plots (M) and quantification (N) are shown ($n = 4$; two-tailed t test). (**O** and **P**) Mice vaccinated with DC-OVA and treated by anti-LAP develop immune memory. (O) Study design. (P) Accumulation of memory-like IL-$7R^+CD44^+$ CD8 T cells in anti-LAP–treated mice by flow cytometry ($n = 4$). Error bars, means ± SEM. One-way ANOVA (D, E, G, H, and P) was used for P value calculations.

In summary, in addition to targeting T_{regs}, our results demonstrate a more complex process because anti-LAP also modulates DCs that express surface LAP, blocks TGF-β, and decreases tolerogenic $CD103^+$ CD8 T cells (fig. S10). Anti-LAP acts on multiple populations to promote antitumor immunity by increasing the activity of $CD8^+$ T effector cells and enhancing immune memory. Consistent with our findings, LAP and CD103 expression in human cancer is associated with a poorer prognosis, providing an important translational link between our results and human disease and making anti-LAP an attractive candidate for cancer immunotherapy.

MATERIALS AND METHODS

Study design

Our objective was to investigate the therapeutic effect of anti-LAP antibody in models of cancer and characterize its effect on immune function. We used mice and primary cells and cell lines to address immunologic mechanism. Cages were randomly assigned to different treatment groups. Tumor size and weight loss were the major factors for ending data collection. All data were included in analysis, although in rare situations, clear outliers were excluded. Experimental replication is indicated in the figure legends. Although the study was not blinded, some in vivo experiments were performed independently by investigators in other laboratories. Data were collected using methods that provide numerical values [calipers, scales, bioluminescence imaging (BLI) for tumor size measurement, flow cytometer for assessing protein expression or cell proliferation, and real-time polymerase chain reaction (PCR) instrument and nSolver digital analyzer for mRNA expression measurement]. Animal preclinical studies were reported in accordance with the ARRIVE guidelines.

Animals

C57BL/6-, BALB/c-, CD4 (*B6.129S2-Cd4^{tm1Mak}/J*)–, and CD8 (*B6.129S2-Cd8a^{tm1Mak}/J*)–deficient 6- to 8-week-old male mice were purchased from the Jackson Laboratory. Foxp3–green fluorescent protein reporter mice were housed in a conventional specific pathogen–free facility at the Harvard Institutes of Medicine. All experiments were carried out in accordance with guidelines prescribed by the Institutional Animal Care and Use Committee of the Harvard Medical School.

Antibody treatments

Mice were treated with either anti-LAP or IC mAbs prepared in PBS. Mouse anti-LAP mAbs were isolated from hybridoma generated in-house. Two clones were used for in vivo treatments: TW7-28G11 (IgG2b) and TW7-16B4 (IgG1). Respective ICs, MPC-11 (IgG2b), MOPC-21 (IgG1), anti-CD103 (clone M290), and anti-PD1 (RMP-1) were purchased from Bio X Cell. As a standard treatment, antibodies (10 mg/kg) were administered intraperitoneally every third day after tumor implantation. In some experiments, mice were treated intraperitoneally with 100 μg of anti-CD8β (clone Lyt-3.2; Bio X Cell) antibody, or IC (rat IgG1; HRPN, Bio X Cell) per mouse on days –1, 7, and 14 after B16F10 implantation.

Statistical analysis

Two-sample *t* test was used to compare two groups, one-way analysis of variance (ANOVA) with Tukey's adjustment for multiple comparisons was used to compare more than two groups, and two-way ANOVA was used to compare two or more groups over time. Survival curves were compared using a log-rank test. A two-sided α level of 0.05 was used for all tests. Analyses were completed using GraphPad Prism version 7.0a. Details of each analysis are included in the source data in the Supplementary Materials.

SUPPLEMENTARY MATERIALS

immunology.sciencemag.org/cgi/content/full/2/11/eaaj1738/DC1

Materials and Methods

Fig. S1. Effects of anti-LAP in tumor models.

Fig. S2. Expression of LAP-associated genes correlates with decreased patient survival in human cancer.

Fig. S3. Analysis of LAP^+ CD4 T cells in the B16 melanoma model.

Fig. S4. Analysis of LAP^+ CD4 T cells in the B16 melanoma model (continued).

Fig. S5. Immune responses by myeloid cells after anti-LAP treatment in cancer models.

Fig. S6. Immune responses after anti-LAP treatment in cancer models.

Fig. S7. Effect of anti-LAP on $CD103^+$ CD8 T cells in cancer models.

Fig. S8. Characterization of $CD103^+$ CD8 T cells in cancer models.

Fig. S9. Anti-LAP treatment combined with antigen-specific vaccination improves immune memory.

Fig. S10. Schematic: Anti-LAP suppresses tumor growth by targeting multiple immune pathways.

Source data (Excel)

References (*51*–*53*)

REFERENCES AND NOTES

1. J. D. Fontenot, M. A. Gavin, A. Y. Rudensky, Foxp3 programs the development and function of $CD4^+CD25^+$ regulatory T cells. *Nat. Immunol.* **4**, 330–336 (2003).
2. S. Hori, T. Nomura, S. Sakaguchi, Control of regulatory T cell development by the transcription factor *Foxp3*. *Science* **299**, 1057–1061 (2003).
3. H. Ochi, M. Abraham, H. Ishikawa, D. Frenkel, K. Yang, A. S. Basso, H. Wu, M. L. Chen, R. Gandhi, A. Miller, R. Maron, H. L. Weiner, Oral CD3-specific antibody suppresses autoimmune encephalomyelitis by inducing $CD4^+$ $CD25^-$ LAP^+ T cells. *Nat. Med.* **12**, 627–635 (2006).
4. M. G. Roncarolo, S. Gregori, M. Battaglia, R. Bacchetta, K. Fleischhauer, M. K. Levings, Interleukin-10-secreting type 1 regulatory T cells in rodents and humans. *Immunol. Rev.* **212**, 28–50 (2006).
5. M.-L. Chen, B.-S. Yan, Y. Bando, V. K. Kuchroo, H. L. Weiner, Latency-associated peptide identifies a novel $CD4^+CD25^+$ regulatory T cell subset with TGFβ-mediated function and enhanced suppression of experimental autoimmune encephalomyelitis. *J. Immunol.* **180**, 7327–7337 (2008).
6. A. P. da Cunha, H. Y. Wu, R. M. Rezende, T. Vandeventer, H. L. Weiner, In vivo anti-LAP mAb enhances IL-17/IFN-γ responses and abrogates anti-CD3-induced oral tolerance. *Int. Immunol.* **27**, 73–82 (2015).
7. M. Scurr, K. Ladell, M. Besneux, A. Christian, T. Hockey, K. Smart, H. Bridgeman, R. Hargest, S. Phillips, M. Davies, D. Price, A. Gallimore, A. Godkin, Highly prevalent colorectal cancer-infiltrating LAP^+ $Foxp3^-$ T cells exhibit more potent immunosuppressive activity than $Foxp3^+$ regulatory T cells. *Mucosal Immunol.* **7**, 428–439 (2014).
8. H.-B. Jie, N. Gildener-Leapman, J. Li, R. M. Srivastava, S. P. Gibson, T. L. Whiteside, R. L. Ferris, Intratumoral regulatory T cells upregulate immunosuppressive molecules in head and neck cancer patients. *Br. J. Cancer* **109**, 2629–2635 (2013).
9. D. A. Thomas, J. Massague, TGF-β directly targets cytotoxic T cell functions during tumor evasion of immune surveillance. *Cancer Cell* **8**, 369–380 (2005).
10. M. A. Travis, D. Sheppard, TGF-β activation and function in immunity. *Annu. Rev. Immunol.* **32**, 51–82 (2014).
11. M. Pickup, S. Novitskiy, H. L. Moses, The roles of TGFβ in the tumour microenvironment. *Nat. Rev. Cancer* **13**, 788–799 (2013).
12. R. Wang, J. Zhu, X. Dong, M. Shi, C. Lu, T. A. Springer, GARP regulates the bioavailability and activation of TGFβ. *Mol. Biol. Cell* **23**, 1129–1139 (2012).
13. D. B. Rifkin, Latent transforming growth factor-β (TGF-β) binding proteins: Orchestrators of TGF-β availability. *J. Biol. Chem.* **280**, 7409–7412 (2005).
14. J. Stockis, D. Colau, P. G. Coulie, S. Lucas, Membrane protein GARP is a receptor for latent TGF-β on the surface of activated human Treg. *Eur. J. Immunol.* **39**, 3315–3322 (2009).
15. T. Oida, H. L. Weiner, TGF-β induces surface LAP expression on murine CD4 T cells independent of Foxp3 induction. *PLOS ONE* **5**, e15523 (2010).
16. Y. Zheng, A. Chaudhry, A. Kas, P. deRoos, J. M. Kim, T.-T. Chu, L. Corcoran, P. Treuting, U. Klein, A. Y. Rudensky, Regulatory T-cell suppressor program co-opts transcription factor IRF4 to control T_H2 responses. *Nature* **458**, 351–356 (2009).
17. M. Zhang, H. Tang, Z. Guo, H. An, X. Zhu, W. Song, J. Guo, X. Huang, T. Chen, J. Wang, X. Cao, Splenic stroma drives mature dendritic cells to differentiate into regulatory dendritic cells. *Nat. Immunol.* **5**, 1124–1133 (2004).

18. S. Song, P. Yuan, H. Wu, J. Chen, J. Fu, P. Li, J. Lu, W. Wei, Dendritic cells with an increased PD-L1 by TGF-β induce T cell anergy for the cytotoxicity of hepatocellular carcinoma cells. *Int. Immunopharmacol.* **20**, 117–123 (2014).
19. M. B. Mokrani, J. Klibi, D. Bluteau, G. Bismuth, F. Mami-Chouaib, Smad and NFAT pathways cooperate to induce CD103 expression in human CD8 T lymphocytes. *J. Immunol.* **192**, 2471–2479 (2014).
20. R. El-Asady, R. Yuan, K. Liu, D. Wang, R. E. Gress, P. J. Lucas, C. B. Drachenberg, G. A. Hadley, TGF-β–dependent CD103 expression by $CD8^+$ T cells promotes selective destruction of the host intestinal epithelium during graft-versus-host disease. *J. Exp. Med.* **201**, 1647–1657 (2005).
21. E. Sefik, N. Geva-Zatorsky, S. Oh, L. Konnikova, D. Zemmour, A. M. McGuire, D. Burzyn, A. Ortiz-Lopez, M. Lobera, J. Yang, S. Ghosh, A. Earl, S. B. Snapper, R. Jupp, D. Kasper, D. Mathis, C. Benoist, Individual intestinal symbionts induce a distinct population of $ROR\gamma^+$ regulatory T cells. *Science* **349**, 993–997 (2015).
22. K. S. Voo, Y.-H. Wang, F. R. Santori, C. Boggiano, Y. H. Wang, K. Arima, L. Bover, S. Hanabuchi, J. Khalili, E. Marinova, B. Zheng, D. R. Littman, Y.-J. Liu, Identification of IL-17-producing $FOXP3^+$ regulatory T cells in humans. *Proc. Natl. Acad. Sci. U.S.A.* **106**, 4793–4798 (2009).
23. P. D. Bos, A. Y. Rudensky, T_{reg} cells in cancer: A case of multiple personality disorder. *Sci. Transl. Med.* **4**, 164fs44 (2012).
24. J. J. Obar, E. R. Jellison, B. S. Sheridan, D. A. Blair, Q.-M. Pham, J. M. Zickovich, L. Lefrancois, Pathogen-induced inflammatory environment controls effector and memory $CD8^+$ T cell differentiation. *J. Immunol.* **187**, 4967–4978 (2011).
25. J. J. Obar, L. Lefrançois, Early signals during $CD8^+$ T cell priming regulate the generation of central memory cells. *J. Immunol.* **185**, 263–272 (2010).
26. J. Reiser, A. Banerjee, Effector, memory, and dysfunctional $CD8^+$ T cell fates in the antitumor immune response. *J. Immunol. Res.* **2016**, 8941260 (2016).
27. C. Liu, C. J. Workman, D. A. A. Vignali, Targeting regulatory T cells in tumors. *FEBS J.* **283**, 2731–2748 (2016).
28. H. Pere, C. Tanchot, J. Bayry, M. Terme, J. Taieb, C. Badoual, O. Adotevi, N. Merillon, E. Marcheteau, V. R. Quillien, C. Banissi, A. Carpentier, F. Sandoval, M. Nizard, F. Quintin-Colonna, G. Kroemer, W. H. Fridman, L. Zitvogel, S. P. Oudard, E. Tartour, Comprehensive analysis of current approaches to inhibit regulatory T cells in cancer. *Oncoimmunology* **1**, 326–333 (2012).
29. J. Mahalingam, Y.-C. Lin, J.-M. Chiang, P.-J. Su, J.-H. Fang, Y.-Y. Chu, C.-T. Huang, C.-T. Chiu, C.-Y. Lin, LAP^+CD4^+ T cells are suppressors accumulated in the tumor sites and associated with the progression of colorectal cancer. *Clin. Cancer Res.* **18**, 5224–5233 (2012).
30. J. Wang, A. Ioan-Facsinay, E. I. van der Voort, T. W. J. Huizinga, R. E. M. Toes, Transient expression of FOXP3 in human activated nonregulatory $CD4^+$ T cells. *Eur. J. Immunol.* **37**, 129–138 (2007).
31. T. Saito, H. Nishikawa, H. Wada, Y. Nagano, D. Sugiyama, K. Atarashi, Y. Maeda, M. Hamaguchi, N. Ohkura, E. Sato, H. Nagase, J. Nishimura, H. Yamamoto, S. Takiguchi, T. Tanoue, W. Suda, H. Morita, M. Hattori, K. Honda, M. Mori, Y. Doki, S. Sakaguchi, Two $FOXP3^+CD4^+$ T cell subpopulations distinctly control the prognosis of colorectal cancers. *Nat. Med.* **22**, 679–684 (2016).
32. G. A. Hadley, S. T. Bartlett, C. S. Via, E. A. Rostapshova, S. Moainie, The epithelial cell-specific integrin, CD103 (alpha E integrin), defines a novel subset of alloreactive $CD8^+$ CTL. *J. Immunol.* **159**, 3748–3756 (1997).
33. K.-L. Ling, N. Dulphy, P. Bahl, M. Salio, K. Maskell, J. Piris, B. F. Warren, B. D. George, N. J. Mortensen, V. Cerundolo, Modulation of CD103 expression on human colon carcinoma-specific CTL. *J. Immunol.* **178**, 2908–2915 (2007).
34. D. Anz, W. Mueller, M. Golic, W. G. Kunz, M. Rapp, V. H. Koelzer, J. Ellermeier, J. W. Ellwart, M. Schnurr, C. Bourquin, S. Endres, CD103 is a hallmark of tumor-infiltrating regulatory T cells. *Int. J. Cancer* **129**, 2417–2426 (2011).
35. J. R. Webb, D. A. Wick, J. S. Nielsen, E. Tran, K. Milne, E. McMurtrie, B. H. Nelson, Profound elevation of $CD8^+$ T cells expressing the intraepithelial lymphocyte marker CD103 (α_E/β_7 integrin) in high-grade serous ovarian cancer. *Gynecol. Oncol.* **118**, 228–236 (2010).
36. F. Djenidi, J. Adam, A. Goubar, A. Durgeau, G. Meurice, V. de Montpreville, P. Validire, B. Besse, F. Mami-Chouaib, $CD8^+CD103^+$ tumor–infiltrating lymphocytes are tumor-specific tissue-resident memory T cells and a prognostic factor for survival in lung cancer patients. *J. Immunol.* **194**, 3475–3486 (2015).
37. Y. Liu, Q. Lan, L. Lu, M. Chen, Z. Xia, J. Ma, J. Wang, H. Fan, Y. Shen, B. Ryffel, D. Brand, F. Quismorio, Z. Liu, D. A. Horwitz, A. Xu, S. G. Zheng, Phenotypic and functional characteristic of a newly identified $CD8^+$ $Foxp3^-$ $CD103^+$ regulatory T cells. *J. Mol. Cell Biol.* **6**, 81–92 (2014).
38. E. Uss, A. T. Rowshani, B. Hooibrink, N. M. Lardy, R. A. W. van Lier, I. J. M. ten Berge, CD103 is a marker for alloantigen-induced regulatory $CD8^+$ T cells. *J. Immunol.* **177**, 2775–2783 (2006).
39. H. Keino, S. Masli, S. Sasaki, J. W. Streilein, J. Stein-Streilein, $CD8^+$ T regulatory cells use a novel genetic program that includes CD103 to suppress Th1 immunity in eye-derived tolerance. *Invest. Ophthalmol. Vis. Sci.* **47**, 1533–1542 (2006).
40. L. Lu, Y. Yu, G. Li, L. Pu, F. Zhang, S. Zheng, X. Wang, $CD8^+CD103^+$ regulatory T cells in spontaneous tolerance of liver allografts. *Int. Immunopharmacol.* **9**, 546–548 (2009).
41. M. Mattoscio, R. Nicholas, M. P. Sormani, O. Malik, J. S. Lee, A. D. Waldman, F. Dazzi, P. A. Muraro, Hematopoietic mobilization: Potential biomarker of response to natalizumab in multiple sclerosis. *Neurology* **84**, 1473–1482 (2015).
42. J. L. Coombes, K. R. Siddiqui, C. V. Arancibia-Carcamo, J. Hall, C.-M. Sun, Y. Belkaid, F. Powrie, A functionally specialized population of mucosal $CD103^+$ DCs induces $Foxp3^+$ regulatory T cells via a TGF-β– and retinoic acid–dependent mechanism. *J. Exp. Med.* **204**, 1757–1764 (2007).
43. O. Annacker, J. L. Coombes, V. Malmstrom, H. H. Uhlig, T. Bourne, B. Johansson-Lindbom, W. W. Agace, C. M. Parker, F. Powrie, Essential role for CD103 in the T cell–mediated regulation of experimental colitis. *J. Exp. Med.* **202**, 1051–1061 (2005).
44. C. L. Scott, A. M. Aumeunier, A. M. Mowat, Intestinal $CD103^+$ dendritic cells: Master regulators of tolerance? *Trends Immunol.* **32**, 412–419 (2011).
45. R. Gandhi, D. E. Anderson, H. L. Weiner, Cutting Edge: Immature human dendritic cells express latency-associated peptide and inhibit T cell activation in a TGF-β-dependent manner. *J. Immunol.* **178**, 4017–4021 (2007).
46. Y. Zhang, R. Morgan, C. Chen, Y. Cai, E. Clark, W. N. Khan, S.-U. Shin, H.-M. Cho, A. Al Bayati, A. Pimentel, J. D. Rosenblatt, Mammary-tumor-educated B cells acquire LAP/TGF-β and PD-L1 expression and suppress anti-tumor immune responses. *Int. Immunol.* **28**, 423–433 (2016).
47. R. M. Rezende, A. P. da Cunha, C. Kuhn, S. Rubino, H. M'Hamdi, G. Gabriely, T. Vandeventer, S. Liu, R. Cialic, N. Pinheiro-Rosa, R. P. Oliveira, J. T. Gaublomme, N. Obholzer, J. Kozubek, N. Pochet, A. M. C. Faria, H. L. Weiner, Identification and characterization of latency-associated peptide-expressing γδ T cells. *Nat. Commun.* **6**, 8726 (2015).
48. M.-L. Chen, B.-S. Yan, D. Kozoriz, H. L. Weiner, Novel $CD8^+$ Treg suppress EAE by TGF-β- and IFN-γ-dependent mechanisms. *Eur. J. Immunol.* **39**, 3423–3435 (2009).
49. E. Cerami, J. Gao, U. Dogrusoz, B. E. Gross, S. O. Sumer, B. A. Aksoy, A. Jacobsen, C. J. Byrne, M. L. Heuer, E. Larsson, Y. Antipin, B. Reva, A. P. Goldberg, C. Sander, N. Schultz, The cBio Cancer Genomics Portal: An open platform for exploring multidimensional cancer genomics data. *Cancer Discov.* **2**, 401–404 (2012).
50. J. Gao, B. A. Aksoy, U. Dogrusoz, G. Dresdner, B. Gross, S. O. Sumer, Y. Sun, A. Jacobsen, R. Sinha, E. Larsson, E. Cerami, C. Sander, N. Schultz, Integrative analysis of complex cancer genomics and clinical profiles using the cBioPortal. *Sci. Signal.* **6**, pl1 (2013).
51. J. R. Ohlfest, B. M. Andersen, A. J. Litterman, J. Xia, C. A. Pennell, L. E. Swier, A. M. Salazar, M. R. Olin, Vaccine injection site matters: Qualitative and quantitative defects in CD8 T cells primed as a function of proximity to the tumor in a murine glioma model. *J. Immunol.* **190**, 613–620 (2013).
52. S. S. Ahuja, In vitro generation of functional human and murine dendritic cells. *Methods Mol. Biol.* **156**, 67–77 (2001).
53. G. K. Smyth, Linear models and empirical Bayes methods for assessing differential expression in microarray experiments. *Stat. Appl. Genet. Mol. Biol.* **3**, Article3 (2004).

Acknowledgments: We thank B. Healy for providing consultation on statistical analysis; A. Anderson, S. Kurtulus, I. Mascanfroni, D. Hu, and C. Baecher-Allan for assistance and helpful discussion; D. Kozoriz for cell sorting; P. C. Gokhale for support with GBM model experiments; and F. von Glen, R. Griffin, V. Kannan, and A. Gurunathan for technical assistance. **Funding:** This work was supported by NIH (R21NS090163 to H.L.W.) and an Innovation Discovery Grant (from Brigham and Women's Hospital to H.L.W.). **Author contributions:** G.G., A.P.d.C., G.M., H.L., R.M.R., V.K., and H.L.W. designed all the experiments. G.G., A.P.d.C., R.M.R., B.K., T.V., N.S., S.R., L.G., P.K., A.J.L., T.M., and M.A.M. performed all the experiments. A.M. analyzed gene expression data. G.G., A.M., and B.K. performed statistical analyses. A.M.C.F., H.L., and V.K. provided input for the manuscript. G.G. and H.L.W. supervised the experiments and wrote the manuscript. **Competing interests:** A patent related to this study has been filed (PCT/US16/13408, titled "Treatment of cancer with anti-LAP monoclonal antibodies," by H.L.W., G.G., and A.P.d.C.). H.L.W. and G.G. are consultants for Tilos Therapeutics Inc., which develops anti-LAP for clinical application. All other authors declare that they have no competing interests.

Submitted 7 September 2016
Resubmitted 14 February 2017
Accepted 20 April 2017
Published 19 May 2017
10.1126/sciimmunol.aaj1738

Citation: G. Gabriely, A. P. da Cunha, R. M. Rezende, B. Kenyon, A. Madi, T. Vandeventer, N. Skillin, S. Rubino, L. Garo, M. A. Mazzola, P. Kolypetri, A. J. Lanser, T. Moreira, A. M. C. Faria, H. Lassmann, V. Kuchroo, G. Murugaiyan, H. L. Weiner, Targeting latency-associated peptide promotes antitumor immunity. *Sci. Immunol.* **2**, eaaj1738 (2017).

Science Immunology
AAAS

Targeting latency-associated peptide promotes antitumor immunity

Galina Gabriely, Andre P. da Cunha, Rafael M. Rezende, Brendan Kenyon, Asaf Madi, Tyler Vandeventer, Nathaniel Skillin, Stephen Rubino, Lucien Garo, Maria A. Mazzola, Panagiota Kolypetri, Amanda J. Lanser, Thais Moreira, Ana Maria C. Faria, Hans Lassmann, Vijay Kuchroo, Gopal Murugaiyan and Howard L. Weiner

*Sci. Immunol.*2, (2017)
doi: 10.1126/sciimmunol.aaj1738

Editor's Summary LAPping up tumor immunoregulationTumors dodge the immune system in part by promoting immune regulatory cells. Gabriely et al. now report that antibodies to latency-associated peptide (LAP), which forms a complex with transforming growth factor-b (TGF-b), reduced tumor growth in multiple cancer models in mice. The authors found that antibodies to LAP decreased numbers of LAP+ regulatory T cells and tolerogenic dendritic cells within the tumor and TGF-b secretion in vitro. Moreover, anti-LAP antibodies decreased numbers of CD103+ CD8+ T cells in lymphoid organs; these cells were then shown to promote tumor growth. Furthermore, combining LAP antibodies with antigen-specific vaccination enhanced both antitumor immune response and immunological memory. Together, these data suggest that targeting LAP may enhance tumor immunotherapy.

Science Immunology (ISSN 2375-2548) publishes new articles weekly. The journal is published by the American Association for the Advancement of Science (AAAS), 1200 New York Avenue NW, Washington, DC 20005.